

# Crustal structure of northern Borneo from VDSS: Implications for subduction termination and the tectonic reconstruction of SE Asia

Harry Telajan Linang<sup>1</sup>, Simone Pilia<sup>2</sup>, Nicholas Rawlinson<sup>1</sup>, Conor Bacon<sup>1</sup>, Amy Gilligan<sup>3</sup>, David Cornwell<sup>3</sup>, and Felix Tongkul<sup>4</sup>

<sup>1</sup>University of Cambridge

<sup>2</sup>Department of Earth and Environmental Sciences, University of Milan-Bicocca, Milan, Italy

<sup>3</sup>University of Aberdeen

<sup>4</sup>Universiti Malaysia Sabah

November 24, 2022

## Abstract

The post-subduction tectonic evolution of northern Borneo, which experienced two sequential subduction episodes of opposite polarity in the Neogene, is still widely debated with first-order questions such as whether the region has been in a state of compression or extension remaining unresolved. We use waveform data recorded from a dense seismic network in northern Borneo to investigate crustal thickness variations through the application of Virtual Deep Seismic Sounding (VDSS). The new results reveal an extensive area of thin crust in central and southeastern Sabah that appears to extend northeast into the Sulu Sea, where rifting initiated. We also compute local earthquake focal mechanisms, which suggest that extension is ongoing, though now dominated by orogen collapse in the NW. Together these results point to the pervasiveness of regional extension tectonics over the last 15-20 Myr and its role in the post-subduction cycle of plate tectonics in SE Asia.

## Hosted file

grl\_supplementary\_htl.docx available at <https://authorea.com/users/549718/articles/603694-crustal-structure-of-northern-borneo-from-vdss-implications-for-subduction-termination-and-the-tectonic-reconstruction-of-se-asia>

1 **Crustal structure of northern Borneo from VDSS: Implications for subduction**  
2 **termination and the tectonic reconstruction of SE Asia**

3  
4 **H. T. Linang<sup>1</sup>, S. Pilia<sup>1,2</sup>, N. Rawlinson<sup>1</sup>, C. A. Bacon<sup>1</sup>, A. Gilligan<sup>3</sup>, D. G. Cornwell<sup>3</sup>, F.**  
5 **Tongkul<sup>4</sup>**

6  
7 <sup>1</sup> Bullard Laboratories, University of Cambridge, Cambridge, UK, <sup>2</sup> Department of Earth and  
8 Environmental Sciences, University of Milan-Bicocca, Milan, Italy, <sup>3</sup> Department of Geology and  
9 Geophysics, University of Aberdeen, Aberdeen, UK, <sup>4</sup> Faculty of Science and Natural Resource,  
10 Universiti of Malaysia Sabah, Kota Kinabalu, Sabah, Malaysia.

11  
12 Corresponding author: Harry Telajan Linang (htal3@cam.ac.uk)

13  
14 **Key Points:**

- 15 • Crustal thickness map of northern Borneo obtained from Virtual Deep Seismic Sounding  
16 (VDSS).
- 17 • Evidence of crustal thinning indicates Sulu Sea extension propagated into northern Borneo  
18 during the late Miocene.
- 19 • Crustal thinning and newly computed focal mechanism solutions underscore the important  
20 role of extension in post-collisional settings.

21 **Abstract**

22 The post-subduction tectonic evolution of northern Borneo, which experienced two sequential  
23 subduction episodes of opposite polarity in the Neogene, is still widely debated with first-order  
24 questions, such as whether the region has been in a state of compression or extension, remaining  
25 unresolved. We use waveform data recorded from a dense seismic network in northern Borneo to  
26 investigate crustal thickness variations through the application of Virtual Deep Seismic Sounding  
27 (VDSS). The new results reveal an extensive area of thin crust in central and southeastern Sabah  
28 that appears to extend northeast into the Sulu Sea, where rifting initiated. We also compute local  
29 earthquake focal mechanisms, which suggest that extension is ongoing, though now dominated by  
30 orogen collapse in the NW. Together these results point to the pervasiveness of regional extension  
31 over the last 15-20 Myr and its role in the post-subduction cycle of plate tectonics in SE Asia.

32

33 **Plain Language Summary**

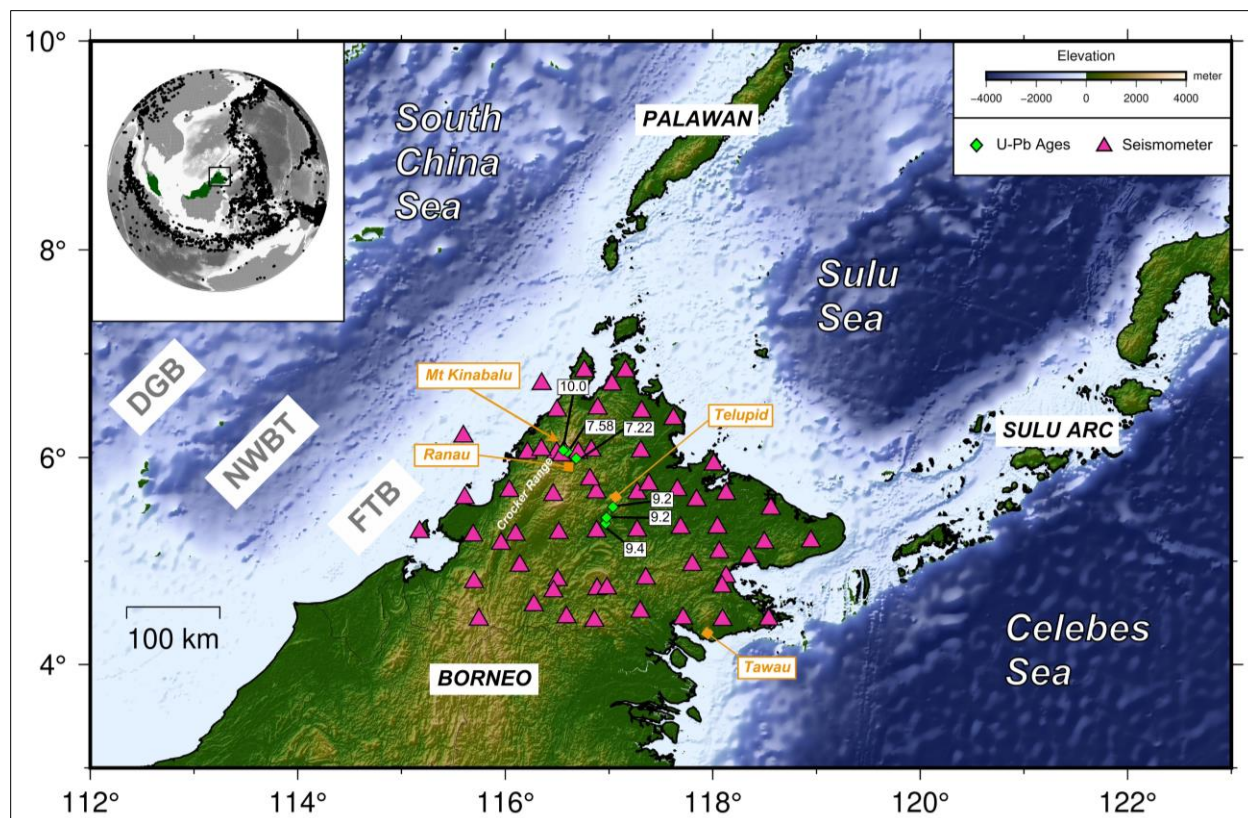
34 Northern Borneo, which lies in the heart of southeast Asia, was assembled by a complex series of  
35 tectonic events over the last 40 million years. Principle among these was subduction of the Proto  
36 South China Sea plate beneath its northwest continental margin, which ended in continent-  
37 continent collision. Subduction of the Celebes Sea plate in the SW followed, which terminated ~  
38 9 million years ago. A key point of debate in the evolution of this region is the relative dominance  
39 of compressional and extensional tectonics. In this study, we exploit seismic data collected in  
40 northern Borneo from a dense array of seismometers to construct a new crustal model of the region,  
41 which robustly constrains the crust-mantle boundary. We find that the crust in central northern  
42 Borneo is anomalously thin and appears to extend NE into the Sulu Sea, which is consistent with  
43 a model of rifting and ocean basin formation that propagated into the adjacent continent. An

44 analysis of earthquake sources also indicate a predominance of normal faulting, which suggests  
45 that extensional tectonics likely dominated the region following the earlier continent-continent  
46 collision. This finding has important implications for understanding both post-collisional and post-  
47 subduction processes and the assembly of Southeast Asia.

48

## 49 **Introduction**

50 Northern Borneo, which incorporates the Malaysian state of Sabah, represents a unique  
51 opportunity to understand the evolution of continental lithosphere in a post-subduction setting, in  
52 this case, produced by sequential termination of two opposed subduction systems in the Miocene,  
53 and holds vital clues for unraveling the complex tectonic history of Southeast Asia (e.g., Rangun,  
54 1990; Hutchison, 2000; Hall, 2008; Hall, 2013; Tongkul, 2017). Subduction of the Proto-South  
55 China Sea (PSCS) beneath NW Sabah began in the Eocene and ceased in the Early Miocene with  
56 continent-continent collision between the Dangerous Grounds block (see Figure 1) and the western  
57 margin of Sabah. Subsequent continental shortening is responsible for deformation and uplift  
58 above sea level of the deep-marine sediments of accretionary complexes such as the Trusmadi and  
59 Crocker Formations (Tongkul, 1991, 1994; Hutchison, 2000, 2005; Hall, 2013, 2017). To the  
60 northeast, the back-arc extension and opening of the Sulu Sea are frequently associated with SE  
61 subduction rollback of the Celebes Sea beneath the Sulu Arc in a time window between ~21 and  
62 ~9 Ma (Hall, 2013; Lai et al., 2020).



63  
 64 **Figure 1. Map of the study area. Magenta triangles show seismic stations from nBOSS and**  
 65 **MetMalaysia networks. Green diamonds denote geochronological dating locations relevant to this**  
 66 **study. Left inset shows the SE Asia region with Malaysia in green and Sabah highlighted by**  
 67 **a black rectangle. DGB, Dangerous Grounds Block; NWBT, NW Borneo Trough; FTB, Fold**  
 68 **and Thrust Belt.**

69  
 70 A unifying narrative describing the tectonic history of Sabah has proven elusive for various  
 71 reasons, including the presence of complex geology masked by thick tropical regolith and  
 72 vegetation, and a lack of information on the crust and underlying mantle structure. From a  
 73 geochronological perspective, reliable data in the region are limited to only a few clusters (Figure  
 74 1); this has prevented previous studies from making robust inferences about significant geological

75 features and properly constraining the timing of key tectonic developments in Sabah's history.  
76 More importantly, the Neogene evolution of northern Borneo and associated neotectonic activity  
77 remains controversial, with most explanations lying between two end-member models: (i)  
78 compressional tectonics, at least partially associated with the opening of the South China Sea  
79 (Tongkul, 1994, 1997; Morley & Back, 2008; Morley et al., 2011) and (ii) extensional tectonics,  
80 predominantly driven by trench retreat of the Celebes Sea (Hall, 2013; Pilia et al., 2021a).

81         Recently, fresh clues have been obtained by Tsikouras et al. (2021) with new zircon  
82 radiometric dating of the Ranau peridotites and Telupid ophiolite in Sabah (Figure 1). They suggest  
83 that back-arc extension propagated from the Sulu Sea into northern Borneo, resulting in significant  
84 extension that led to the exhumation of a subcontinental peridotite suite near Ranau and a rift-  
85 related magmatic episode (9.2 to 10.5 Ma) near Telupid. However, this study was subsequently  
86 questioned by Cullen and Burton-Johnson (2021), who argue against the interpretation of the new  
87 zircon ages by Tsikouras et al. (2021) and the possible extent of propagation of Sulu Sea extension  
88 into northern Borneo.

89         Earthquake data recorded by a new, dense seismic network in Sabah represents an excellent  
90 opportunity to constrain many first-order crustal parameters, including thickness and stress  
91 orientation. In this study, we estimate Moho depths by exploiting a recently developed passive  
92 seismic method commonly referred to as Virtual Deep Seismic Sounding (VDSS), initially  
93 proposed by Tseng et al. (2009). We implemented the method as in Thompson et al. (2019) and  
94 Pilia et al. (2021b) to get estimates on the crustal thickness beneath the seismic network in northern  
95 Borneo. At the same time, we infer the present-day distribution of stress from new focal  
96 mechanism analysis of local earthquakes. We then reconcile both sets of results with prior evidence  
97 for either a compressional or extensional tectonic setting in northern Borneo.

## 98 **2 Data Analysis**

### 99 2.1 Virtual Deep Seismic Sounding

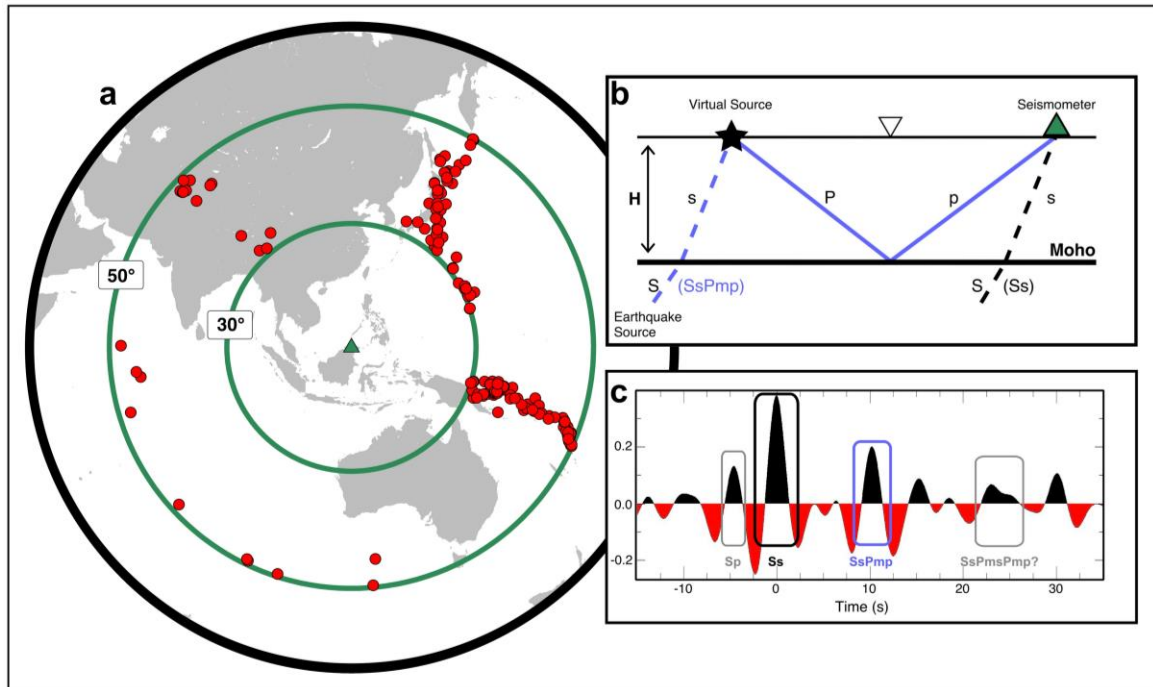
100 We use waveform data recorded by 46 broadband stations of the northern Borneo Orogeny  
101 Seismic Survey (nBOSS) temporary seismic network and 20 broadband stations operated by the  
102 Malaysian Meteorological Department (MetMalaysia) (Pilia et al., 2019) – see Figure 1 for  
103 locations. We use earthquake events with magnitudes larger than 5.0 in an epicentral distance  
104 range between 30° and 50° from the station (Figure 2), resulting in a total of 172 seismic sources.  
105 VDSS focuses on the SsPmp phase, originating from an S-to-P conversion under a free surface.  
106 The converted P-wave then travels downwards and undergoes a wide-angle (post-critical)  
107 reflection at the Moho before impinging on a seismic station (Figure 2). The difference in arrival  
108 time between the SsPmp phase and the Ss phase provides an estimate of the Moho depth through  
109 the following equation:

110

$$111 T_{\text{SsPmp} - \text{Ss}} = 2H (V_p^{-2} - p^2\beta)^{1/2}, \quad (1)$$

112

113 where  $H$  is the crustal thickness,  $V_p$  is the average P-wave speed in the crust, and  $p_\beta$  is the ray  
114 parameter, which is determined using the known source-receiver geometry and the ak135 velocity  
115 model (Kennett et al., 1995).



116

117 **Figure 2. (A) Seismic source distribution (red dots) in the epicentral distance range  $30^{\circ} - 50^{\circ}$**   
 118 **from which earthquake data were extracted. (B) The schematic ray diagram illustrates the**  
 119 **main phases used during the VDSS analysis. (C) An example of stacked waveform data from**  
 120 **a station in Sabah with the Ss and SsPmp arrivals highlighted in black and blue, respectively.**  
 121 **The precursor Sp phase and reverberatory SsPmsPmp are also labeled and highlighted in**  
 122 **grey.**

123

124 The first step in preparing a VDSS trace is to isolate the SsPmp phase from its event  
 125 waveform. This involves windowing data around the S-arrival time generated by a teleseismic  
 126 source, using predictions from a global reference model (ak135 in this case). The instrument  
 127 response is then deconvolved from the raw data before applying a second-order zero-phase  
 128 Butterworth bandpass filter with 0.05 Hz and 0.5 Hz corner frequencies. The horizontal  
 129 components are subsequently rotated into the radial and tangential components (Thompson et al.,

130 2019). In order to remove source-side scattering effects, we applied the source normalization  
131 method of Yu et al. (2013), which ultimately allows the use of all seismic events within the  
132 prescribed epicentral distance range regardless of focal depth. This increases the number of viable  
133 waveforms, which is advantageous because the usable epicentral-distance range intrinsic to the  
134 method is limited (Figure 2a).

135 Next, the vertical and radial component traces are rotated into the pseudo-S component  
136 traces (Parker et al., 2016; Thompson et al., 2019). These are then deconvolved from the vertical  
137 and radial component of the waveform using an extended-time multitaper approach (10 s sliding  
138 window, 75% window overlap, 3 Slepian tapers; Helffrich, 2006). The resulting vertical  
139 component VDSS traces are then visually inspected and are retained if: (i) the SsPmp phase is  
140 clearly visible; ii) a prominent direct Ss arrival and precursor sP can be detected; and iii) ringy or  
141 oscillatory signals are absent. Finally, we use the results from a joint receiver function (RF) and  
142 surface wave inversion analysis to produce synthetic seismograms to get the predicted travel time  
143 of the SsPmp phase for different slowness at each station (Pilia et al., 2021b). Thus, the retained  
144 traces (observed data) go through a final inspection where traces are kept if its SsPmp arrival falls  
145 within 4-seconds before and after the predicted zero-crossing of the SsPmp in the synthetic  
146 seismograms.

147 At this stage, the only unknown parameter required to estimate the thickness of the crust  
148 from Equation (1) is the bulk velocity  $V_p$  (Figure S1), which we determined from the joint RF  
149 analysis presented in Pilia et al. (2021a). The S-wave velocities estimated beneath each station  
150 obtained from the RF analysis are converted to P-wave velocities using the empirical relation  
151 devised by Brocher (2005). For each station, we perform a time-to-depth migration of each VDSS  
152 trace based on Equation (1) and linearly stack them to produce a final VDSS trace from which the

153 crustal thickness beneath a station is estimated to be the point where the SsPmp zero-crossing  
154 occurs (Pilia et al., 2021b, Tseng et al., 2009, Yu et al., 2016). Due to the post-critical reflection  
155 of the P-wave at the Moho, SsPmp undergoes a phase shift, in addition to a clear moveout (Figure  
156 S2), that varies across the slowness range between 14.2 and 15.7 sec/deg. The stacking of traces  
157 and good slowness coverage of our data averages out any bias that the phase shift might introduce.  
158 Calculating the envelope function of the single VDSS traces would remove the phase shift;  
159 however, Thompson et al. (2019) show that the zero-crossing proxy and envelope function results  
160 are consistent when a good slowness coverage is present, as it is in our case.

161 The joint RF and surface wave inversion works well in many parts of Sabah but proved  
162 challenging, particularly from the perspective of extracting Moho depths, in the east due to the  
163 extensive sedimentary basins and the presence of shallow ophiolite cover. The higher frequency  
164 content (e.g., 0.05 to 2 Hz) used by RFs appears to be more contaminated by short period noise  
165 and reverberations such that the primary phase Ps is not easily identifiable (Figure S3). For VDSS,  
166 the primary phase SsPmp recorded in eastern Sabah is more discernible due to the low-frequency  
167 content inherent to the method (0.05 to 0.5 Hz), which suppresses undesirable signals arising from  
168 small-scale intra-crustal structure beneath Sabah (Figure S4).

169

## 170 2.2 Analysis of Seismicity

171 We manually picked P-wave first break polarities for 101 earthquakes ( $M_w \geq 2.0$ ) from a  
172 new earthquake catalog for the region around Mt Kinabalu, which were used to calculate moment  
173 tensor solutions (Bacon, 2021). This task was performed using the Bayesian moment tensor  
174 inversion software MTfit by Pugh (2018), wherein we constrained the solutions to be purely  
175 double-couple. MTfit employs a Markov-chain Monte-Carlo approach to explore the posterior

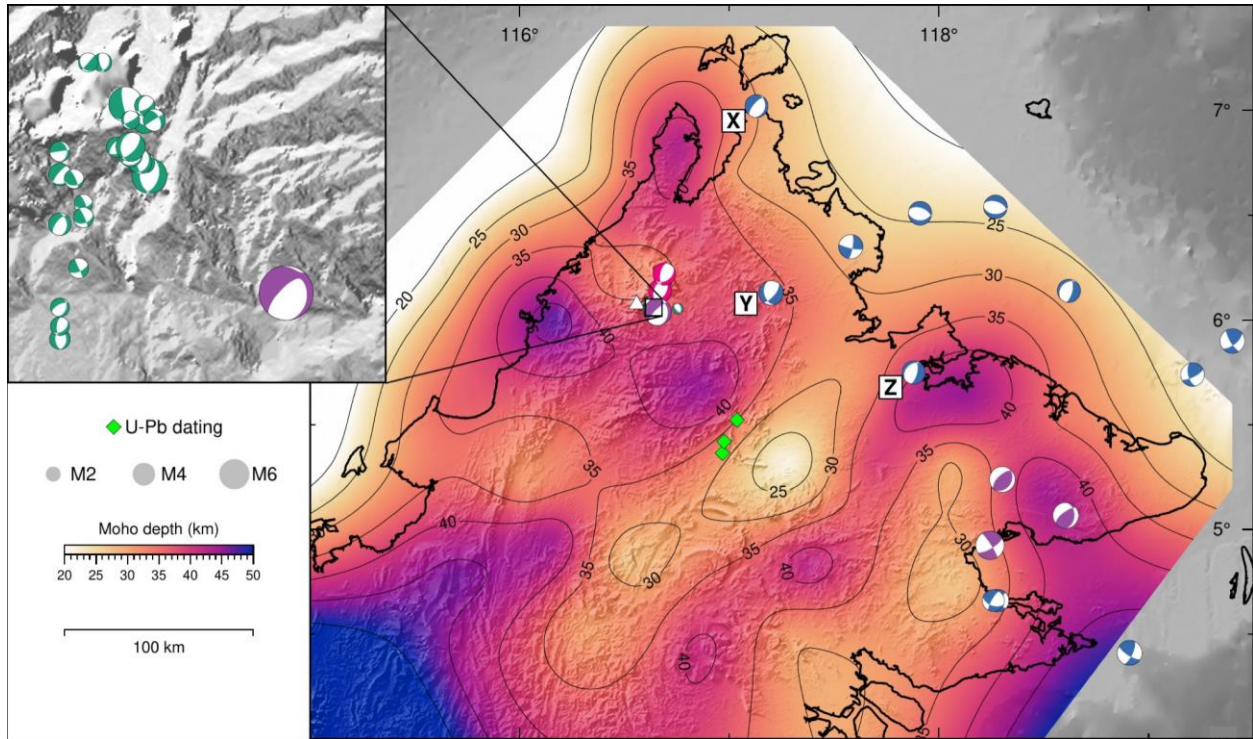
176 probability space and identify the best-fitting moment tensor solution while naturally incorporating  
177 the measurement uncertainties associated with moment tensor estimation (e.g., location and  
178 velocity model uncertainties), which can be significant in the case of microseismicity (Figure S5).  
179 From the 101 earthquakes analyzed, we produce 26 well-constrained moment tensor solutions  
180 (inset in Figure 3; Table S1). These new observations are supplemented by moment tensor  
181 solutions recorded in global catalogs (gCMT, ISC-GEM, and GEOFON), reflecting the broader  
182 history of seismicity recorded across northern Borneo.

183

### 184 **3 Crustal thickness variations in Sabah**

185 Figure 3 illustrates the final Moho-depth map of Sabah obtained using the VDSS method,  
186 which reveals several alternating thin and thick crustal bands, with depths ranging between 21 and  
187 46 km. When compared to crustal thicknesses derived from RF analysis (Pilia et al., 2021a) and  
188 inferred from the shear wave velocity structure (Greenfield et al., 2022), all three results appear  
189 broadly consistent. VDSS has the advantage of obtaining robust depth estimates in the east, where  
190 a clear Moho was absent in the RF results (see Figure S6-7). Inferring Moho depth from a shear-  
191 wave model constrained by surface waves at best constrains the broadscale pattern of Moho depth,  
192 but at least these are largely in agreement with the first-order variations present in the new VDSS  
193 model. The robustness of the VDSS results was investigated by constructing Moho maps using the  
194 SsPmp bounce points at the Moho as the depth measurement location for different subsets of events  
195 (see Figure S8, S9, and S10) and varying the input crustal velocity model by adding random noise

196 (Figure S11). Overall, our analysis suggests that the features that we interpret are well-constrained  
 197 by the data.



198  
 199 **Figure 3. Moho-depth map of Sabah using a color scale centered on 35 km. Green diamonds**  
 200 **show the locations of ophiolites of late Miocene age, as inferred by Tsikouras et al. (2021).**  
 201 **The white triangle denotes Mt Kinabalu. Black lines are depth-to-Moho contours drawn**  
 202 **every 5 km. The top-left inset is a zoom-in of the area around Mt Kinabalu, taken from the**  
 203 **area within the square box. Purple focal mechanisms are gCMT solutions, blue are ISC**  
 204 **solutions, and red are GEOFON solutions. Green focal mechanisms in the inset map are**  
 205 **earthquakes in a new local catalog of seismicity derived from P phase first-motion polarities**  
 206 **at stations in the nBOSS and MetMalaysia networks. Focal mechanisms are represented as**  
 207 **beachball plots, scaled by magnitude (scale factor of 2 for inset map).**

208

209           Following the cessation of PSCS subduction, continent-continent collision occurred in  
210 western Sabah, deforming and elevating much of the Crocker Range. The most abrupt deflection  
211 of the Moho topography inferred by our results appears to coincide with the Crocker Range, where  
212 crustal thickness estimates exceed 40 km in places (Figure 3). This observation suggests that  
213 folding and thrusting due to continent-continent collision between western Sabah and the  
214 Dangerous Grounds has produced a thicker crust with a substantial root beneath the mountain belt  
215 along the western coast. Immediately offshore to the west of the Crocker Range on the continental  
216 shelf (thrust and fold belt), the crust is significantly thinner, a result largely compatible with Moho  
217 depth inferences made from offshore active seismic methods (Franke et al., 2008).

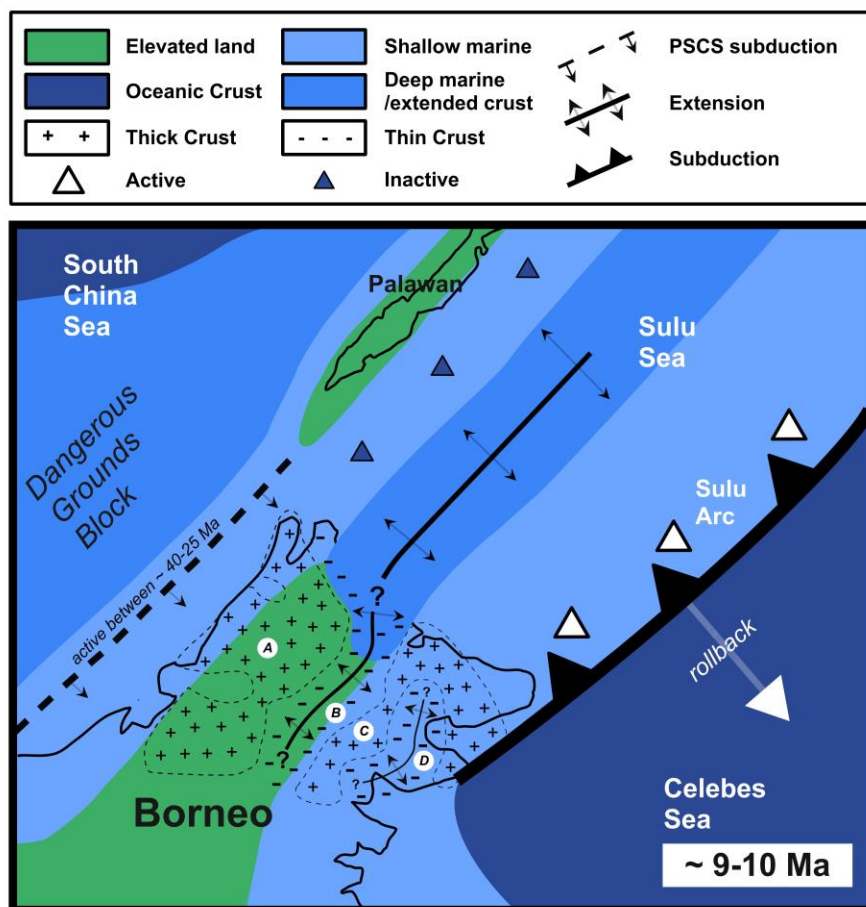
218           A significant result that emerges from this study is the area of thin crust that runs from the  
219 northeast to the southwest in central Sabah (crust B in Figure 4), with a strike resembling that of  
220 the Crocker Range and the NW margin of Sabah. The thin crust is wider at the northeast coast and  
221 appears to continue offshore into the Sulu Sea. New radiometric data from Tsikouras et al. (2021)  
222 indicate that the chemical signature of the Telupid ophiolite represents that of a narrow oceanic  
223 basin. The zircons from the ophiolite are Miocene in age (9.2 to 10 Ma), which is consistent with  
224 the timing of back-arc extension induced by slab rollback of the Celebes Sea. Intriguingly, the area  
225 of thin crust inferred by our results correlates with the mapped exposure of the Telupid ophiolite  
226 and the zircon samples analyzed by Tsikouras et al. (2021). We interpret this area of thin crust as  
227 evidence of Miocene extension tectonics likely related to the same back-arc extension that formed  
228 the Sulu Sea. Brun et al. (2016) suggest that an acceleration in trench retreat in the Aegean changed  
229 the extension mode from localized to distributed. Northern Borneo might have experienced a  
230 similar episode during a period of rapid trench rollback of the Celebes Sea ~16 Ma, as suggested

231 by Hall (2013). During this time, extension in the Sulu Sea might have propagated to the SW, thus  
232 forming the areas of thin crust we observe in Sabah.

233 In the eastern half of Sabah, the Moho depth map reveals an alternating thick and thin  
234 crustal pattern (Figure 3). Despite being narrower than the thick crust labeled A in Figure 4, crust  
235 C similarly displays Moho depths of more than 40 km along its strike (see Figure 4). Further  
236 southeast, the thin crust that underlies the Tawau area (crust D in Figure 4) could have also resulted  
237 from back-arc extension. The overall pattern of an alternating thick and thin crust in Sabah with a  
238 common strike is consistent with extensional tectonics where strain localization produces thinner  
239 crust between thicker and presumably more resistant blocks, somewhat akin to the style of crustal-  
240 scale boudinage observed in the Aegean (Jolivet et al., 2004).

241 The analysis of focal mechanisms observed in Figure 3 provides insight into the present  
242 day stress regime in Sabah. A standout feature of the focal mechanism map is that nearly every  
243 mechanism is either normal or exhibits a clear extensional component in central and western Sabah  
244 (Figure S12). This is not limited to the Ranau area, as indicated by focal mechanisms X, Y, and Z  
245 (see Figure 3), adjacent to the thin crustal region in central Sabah revealed by our new Moho depth  
246 map. We hypothesize that the western half of Sabah is currently undergoing extension, likely  
247 related to orogen collapse, as also suggested by Sapin et al. (2013) based on GPS measurements  
248 and study of the NW Borneo Wedge. The orogen collapse may also drive the active fold and thrust  
249 belt (FTB) structure observed between the NW Borneo Trough and the Crocker Range (Hall,  
250 2013). On the other hand, the east and southeast exhibit more varied focal mechanisms. This could  
251 be related to the reorientation of the Celebes Sea tectonic plate, which is now actively subducting  
252 southward under Sulawesi.

253

254 **4. Conclusion**

255  
 256 **Figure 4.** A sketch of the proposed tectonic evolution of northern Borneo (adapted from Hall,  
 257 **2013; Tsikouras et al., 2021).** A and C represent areas of relatively thick crust, while B and  
 258 **D** represent areas of relatively thin crust.

259  
 260 Our new crustal thickness model of Sabah, derived from applying the VDSS method to  
 261 teleseismic waveform data, is consistent with the operation of extensional tectonics throughout  
 262 much of the Miocene, during which back-arc spreading resulted in the opening of the Sulu Sea.  
 263 The pattern of trench-parallel thick and thin crust in eastern Sabah is reminiscent of crustal-scale  
 264 boudinage structures observed elsewhere during subduction rollback and aligns with

265 interpretations of geochemical and geological data that suggests that Sulu Sea extension  
266 propagated into Sabah in the Miocene. Although we cannot rule out the possibility that these  
267 crustal thickness variations were present prior to the Sulu Sea opening or were influenced by  
268 subsequent events, the confluence of evidence favors extensional rather than compressional  
269 tectonics. Our analysis of new and existing focal mechanisms from local earthquakes supports the  
270 contemporary stress field being extensional, at least in central and western Sabah, albeit through a  
271 different mechanism (orogen collapse) than that invoked for the Miocene. These results show that  
272 crustal extension plays an important role in the evolution of post-subduction continental margins,  
273 even in the circumstances as complex as northern Borneo, where subduction, continent-continent  
274 collision, back-arc extension and orogen collapse have come together to produce a distinctive  
275 chain of events.

276

## 277 **Acknowledgments**

278 We thank MetMalaysia for allowing access to their restricted data. H.T.L. acknowledges the  
279 fieldwork grant awarded by the University of Cambridge through the LWA Research Fund and St  
280 Edmunds' Cherry Hume Prize. S.P. acknowledges support from the Natural Environmental  
281 Research Council (NERC) Grant NE/R013500/1 and from the European Union's Horizon 2020  
282 research and innovation program under Marie Skłodowska-Curie Grant Agreement 790203. We  
283 thank the NERC Geophysical Equipment for loan 1038. Seismic data from the nBOSS network  
284 will be accessible through the IRIS Data Management (<http://www.iris.edu/mda>) from February  
285 2023 (see [https://doi.org/10.7914/SN/YC\\_2018](https://doi.org/10.7914/SN/YC_2018)). Waveform data recorded by the northern Borneo  
286 Orogeny Seismic Survey network were extracted, quality checked, and archived by C. A. Bacon.  
287 Details on the status of this database may be obtained from N.R.

288

289 **Open Research**

290 The waveform data (VDSS traces) for each station can be downloaded from  
291 10.5281/zenodo.6338668. Data analysis was carried out using C Shell and Python (3.7). The  
292 following Python packages were used: ObsPy (1.2.2, Beyreuther et al., 2010) and Numpy (1.21.3,  
293 Harris et al., 2020). Data visualization were performed using Generic Mapping Tools (6.0, Wessel  
294 et al., 2019) and Matplotlib (3.4.3, Hunter, 2007).

295

296 **References**

297 Brocher, T. M. (2005). Empirical relations between elastic wavespeeds and density in the earth's  
298 crust. *Bulletin of the Seismological Society of America*, 95(6), 2081–2092.  
299 <https://doi.org/10.1785/0120050077>

300

301 Bacon, C. A. (2021). Seismic anisotropy and microseismicity: from crustal formation to  
302 subduction termination, (Doctoral thesis). Retrieved from Apollo Repository.  
303 (<https://doi.org/10.17863/CAM.82196>). Cambridge: University of Cambridge.

304

305 Beyreuther, M., Barsch, R., Krischer, L., Megies, T., Behr, Y., & Wassermann, J. (2010). ObsPy:  
306 A Python toolbox for seismology. *Seismological Research Letters*, 81(3), 530-533,  
307 <https://doi.org/10.1785/gssrl.81.3.530>

308

309

310

- 311 Brun, J., Faccenna, C., Gueydan, F., Sokoutis, D., Philippon, M., Kydonakis, K., & Gorini, C.  
312 (2016). The two-stage Aegean extension, from localized to distributed, a result of slab  
313 rollback acceleration. *Canadian Journal of Earth Sciences*, 53, 1142–1157.  
314 <https://doi.10.1139/cjes-2015-0203>  
315
- 316 Cullen, A., & Burton-Johnson, A. (2021). New zircon radiometric U-Pb ages and Lu-Hf isotopic  
317 data from the ultramafic-mafic sequences of Ranau and Telupid (Sabah, eastern Malaysia):  
318 Time to reconsider the geological evolution of Southeast Asia?. *Comment: Geology*, 49,  
319 e541, <https://doi.org/10.1130/G49414C.1>  
320
- 321 Franke, D., Barckhausen, U., Heyde, I., Tingay, M., & Ramli, N. (2008). Seismic images of a  
322 collision zone offshore NW Sabah/Borneo. *Marine and Petroleum Geology*, 25, 606–624,  
323 <https://doi:10.1016/j.marpetgeo.2007.11.004>  
324
- 325 Greenfield, T., Gilligan, A., Pilia, S., Cornwell, G. D., Tongkul, F., Widiyantoro, S., & Rawlinson,  
326 N. (2022). Post-subduction tectonics of Sabah, northern Borneo, inferred from surface  
327 wave tomography. *Geophysical Research Journals, Solid Earth*, 49(3),  
328 <http://doi.org/10.1029/2021GL096117>  
329
- 330 Hall, R. (1996). Reconstructing Cenozoic SE Asia, in Hall, R., and Blundell, D., eds., Tectonic  
331 Evolution of Southeast Asia. *Geological Society, London, Special Publication 106*, 153–  
332 184, <https://doi:10.1144/GSL.SP.1996.106.01.11>  
333

- 334 Hall, R., van Hattum, M.W.A., & Spakman, W. (2008). Impact of India-Asia collision on SE Asia.  
335 The record in Borneo: *Tectonophysics*, 451, 366–389, [https://doi:10.1016/j.tecto.2007.11.](https://doi:10.1016/j.tecto.2007.11.058)  
336 058  
337
- 338 Hall, R. (2013). Contraction and extension in northern Borneo driven by subduction rollback.  
339 *Journal of Asian Earth Sciences*, 76, 399–411, <http://doi:10.1016/j.jseaes.2013.04.01>  
340
- 341 Hall, R., & Spakman, W. (2015). Mantle structure and tectonic history of SE Asia. *Tectonophysics*,  
342 <https://doi:10.1016/j.tecto.2015.07.003>  
343
- 344 Hall, R., & Breithfeld, H.T. (2017). Nature and demise of the Proto-South China Sea. *Bulletin of*  
345 *the Geological Society of Malaysia*, 63, 61–76, <https://doi:10.7186/bgsm63201703>  
346
- 347 Harris, C. R., Millman, K. J., van der Walt, S. J., Gommers, R., Virtanen, P., Cournapeau, D., et  
348 al. (2020). Array programming with NumPy. *Nature*, 585(7825), 357-362,  
349 <https://doi.org/10.1038/s41586-020-2649-2>  
350
- 351 Helffrich, G. (2006). Extended-time multitaper frequency domain cross-correlation receiver-  
352 function estimation. *Bulletin of the Seismological Society of America*, 96, 344–347,  
353 <https://doi:10.1785/0120050098>  
354
- 355 Hunter, J. D (2007). Matplotlib: A 2D graphics environment. *Computing in Science &*  
356 *Engineering*, 9(3), 90-95, <https://doi.org/10.1109/MCSE.2007.55>

357 Hutchison, C.S. (2005). Geology of north-west Borneo. *Elsevier*, 351-356,  
358 <https://doi.org/10.1016/B978-0444519986/50028-4>

359

360 Hutchison, C.S., Bergman, S.C., Swauger, D.A., & Graves, J.E. (2000). A Miocene collisional belt  
361 in north Borneo. Uplift mechanism and isostatic adjustment quantified by  
362 thermochronology. *Journal of the Geological Society*, 157, 783–793,  
363 <https://doi:10.1144/jgs.157.4.783>

364

365 Jolivet, L., Famin, V., Mehl, C., Parra, T., Aubourg, C., Hebert, R., & Philippot, P. (2004). Strain  
366 localization during crustal-scale boudinage to form extensional metamorphic domes in the  
367 Aegean Sea. *Geological Society of London Special Publication*, 380, 185–210,  
368 <https://doi.org/10.1130/0-8137-2380-9.185>

369

370 Kennett, B.L.N., Engdahl, E.R., & Buland, R. (1995). Constraints on seismic velocities in the Earth  
371 from traveltimes. *Geophysical Journal International*, 122, 108–124,  
372 <https://doi:10.1111/j.1365-246X.1995.tb03540.x>

373

374 Lai, C.K., Xia, X.P., Hall, R., Meffre, S., Tsikouras, B., Rosana Balangue-Tarriela, M.I., Idrus, A.,  
375 Ifandi, E., & Norazme, N. (2021). Cenozoic evolution of the Sulu Sea Arc-basin system.  
376 An overview. *Tectonics*, 40, 1–26, <https://doi:10.1029/2020TC006630>

377

378 Morley, C.K., & Back, S. (2008). Estimating hinterland exhumation from late orogenic basin  
379 volume, NW Borneo. *Journal of the Geological Society*, 165, 353–366,  
380 <https://doi.org/10.1144/0016-76492007-067>

381  
382 Morley, C.K., King, R., Hillis, R., Tingay, M., & Backe, G. (2011). Deepwater fold and thrust belt  
383 classification, tectonics, structure and hydrocarbon prospectivity. A review: *Earth-Science*  
384 *Reviews*, 104, 41–91, <https://doi:10.1016/j.earscirev.2010.09.010>

385  
386 Parker, E. H., Hawman, R. B., Fischer, K. M. & Wagner, L.S. (2016). Estimating crustal thickness  
387 using SsPmp in regions covered by low-velocity sediments: imaging the Moho beneath the  
388 Southeastern Suture of the Appalachian Margin Experiment (SESAME) array, SE Atlantic  
389 Coastal Plain. *Geophysical Research Letters*. 43(18), 9627-9635,  
390 <https://doi.org/10.1002/2016GL070103>

391  
392 Pilia, S., Davies, D.R., Hall, R., Bacon, C., Gilligan, A., Greenfield, et. al. (2021a). Effects of post-  
393 subduction processes on continental lithosphere. [https://doi.org/10.21203/rs.3.rs-](https://doi.org/10.21203/rs.3.rs-861968/v1)  
394 [861968/v1](https://doi.org/10.21203/rs.3.rs-861968/v1)

395  
396 Pilia, S., Rawlinson, N., Gilligan, A., & Tongkul, F. (2019). Deciphering the fate of plunging  
397 tectonic plates in Borneo. *Eos, Transactions American Geophysical Union* 100, 18-23,  
398 <https://doi.org/10.1029/2019EO123475>

399

- 400 Pilia, S., Ali, M.Y., Searle, M.P., Watts, A.B., Lü, C., & Thompson, D.A. (2021b). Crustal  
401 structure of the UAE-Oman mountain range and Arabian rifted passive margin: New  
402 constraints from active and passive seismic methods. *Journal of Geophysical Research,*  
403 *Solid Earth*, 126, <https://doi:10.1029/2020JB021374>  
404
- 405 Pugh, D.J., & White, R. S. (2018). MTfit: A Bayesian Approach to Moment Tensor Inversion.  
406 *Seismological Research Letters*, 89, 1507–1513, <https://doi.org/10.1785/0220170273>  
407
- 408 Rangin, C., Jolivet, L., & Pubellier, M. (1990). A simple model for the tectonic evolution of  
409 Southeast Asia and Indonesia region for the past 43 m.y. *Bulletin de la Société Géologique*  
410 *de France*, 6, 889–905, <https://doi.org/10.2113/gssgfbull.VI.6.889>  
411
- 412 Sapin, F., Hermawan, I., Pubellier, M., Vigny, C., & Ringenbach, J-C. (2013). The recent  
413 convergence on the NW Borneo Wedge. A crustal-scale gravity gliding evidenced from  
414 GPS. *Geophysical Journal International*, 193, 549-556, <https://doi:10.1093/gji/ggt054>  
415
- 416 Thompson, D.A., Rawlinson, N., & Tkalčić, H. (2019). Testing the limits of virtual deep seismic  
417 sounding via new crustal thickness estimates of the Australian continent. *Geophysical*  
418 *Journal International*, 218, 797–800, <https://doi:10.1093/gji/ggz191>  
419
- 420 Tongkul, F. (1991). Tectonic evolution of Sabah, Malaysia. *Journal of Southeast Asian Earth*  
421 *Sciences*, 6, 395–405, [https://doi:10.1016/0743-9547\(91\)90084-B](https://doi:10.1016/0743-9547(91)90084-B)  
422

- 423 Tongkul, F. (1994). The geology of Northern Sabah, Malaysia: Its relationship to the opening of  
424 the South China Sea Basin. *Tectonophysics*, 235, 131–147, [https://doi:10.1016/0040-](https://doi:10.1016/0040-1951(94)90021-3)  
425 1951(94)90021-3  
426
- 427 Tongkul, F. (1997). Polyphase deformation in the Telupid area, Sabah, Malaysia. *Journal of Asian*  
428 *Earth Sciences*, 15, 175–183, [https://doi.org/10.1016/S0743-9547\(97\)00006-8](https://doi.org/10.1016/S0743-9547(97)00006-8)  
429
- 430 Tseng, T.L., Chen, W.P., & Nowack, R.L. (2009). Northward thinning of Tibetan crust revealed  
431 by virtual seismic profiles. *Geophysical Research Letters*, 36, 1–5,  
432 <https://doi:10.1029/2009GL040457>  
433
- 434 Tsikouras, B., La, C.K., Ifandi, E., Norazme, N.A., Teo, C.H., & Xia, X.P. (2021). New zircon  
435 radiometric U-Pb Ages and Lu-Hf isotopic data from the ultramafic-mafic sequences of  
436 Ranau and Telupid (Sabah, East Malaysia): Time to reconsider the geological evolution of  
437 Southeast Asia? *Geology*, 49, 789–793, <https://doi:10.1130/G48126.1>  
438
- 439 Wessel, P., Luis, J., Uieda, L., Scharroo, R., Wobbe, F., Smith, W., & Tian, D. (2019). The Generic  
440 Mapping Tools version 6. *Geochemistry, Geophysics, Geosystems*, 20(11), 5556–5564,  
441 <https://doi.org/10.1029/2019GC008515>  
442
- 443 Yu, C.Q., Chen, W.P., & van der Hilst, R.D. (2013). Removing source-side scattering for virtual  
444 deep seismic sounding (VDSS). *Geophysical Journal International*, 195, 1932–1941,  
445 <https://doi:10.1093/gji/ggt359>